High-strength silk protein scaffolds for bone repair

Biman B. Mandal[a,b], Ariela Grinberg[a,c], Eun Seok Gil[a], Bruce Panilaitis[a], and David L. Kaplan[a,1]

[a]Department of Biomedical Engineering, Tufts University, 4 Colby Street, Medford, MA 02155; [b]Department of Biotechnology, Indian Institute of Technology, Guwahati 781039, India; and [c]Department of Tissue Engineering, Cell Therapy and Regenerative Medicine, National Institute of Rehabilitation, 14389 Mexico D.F., Mexico

Edited by Gregory A. Petsko, Brandeis University, Waltham, MA, and approved March 20, 2012 (received for review December 13, 2011)

Biomaterials for bone tissue regeneration represent a major focus of orthopedic research. However, only a handful of polymeric biomaterials are utilized today because of their failure to address critical issues like compressive strength for load-bearing bone grafts. In this study development of a high compressive strength (~13 MPa hydrated state) polymeric bone composite materials is reported, based on silk protein-protein interfacial bonding. Micron-sized silk fibers (10–600 μm) obtained utilizing alkali hydrolysis were used as reinforcement in a compact fiber composite with tunable compressive strength, surface roughness, and porosity based on the fiber length included. A combination of surface roughness, porosity, and scaffold stiffness favored human bone marrow-derived mesenchymal stem cell differentiation toward bone-like tissue in vitro based on biochemical and gene expression for bone markers. Further, minimal in vivo immunomodulatory responses suggested compatibility of the fabricated silk-fiber-reinforced composite matrices for bone engineering applications.

microfibers | composite scaffold | tissue engineering | osteogenesis | regenerative medicine

Bone defects, both large and small, from nonunions or trauma, pose a significant challenge and often require surgical intervention (1). In the United States alone, 1.3 million people undergo bone graft surgeries each year for skeletal defects either from accidents or disease (2). However, current treatments mostly rely on autografts or allografts but have associated risks, with autografts needing an additional surgical site and limits to supply, and allografts having potential risks of disease transmission and long-term complications (3, 4).

Tissue engineering represents a promising solution toward repair and replacement of these diseased and damaged bone tissues with engineered grafts. Toward this goal, a wide range of natural and synthetic biodegradable polymers has been investigated, including hyaluronic acid, chitosan, poly(L-lactide-co-glycolide) (PLGA), polycaprolactone (PCL), and polymethylmethacrylate (PMMA), as well as several ceramic materials such as calcium phosphate, calcium sulfate, and bioactive glass (5–10). Each of these materials presents limitations in achieving the requirements for bone repair scaffolds.

To improve on the mechanical properties and osteoinductive potential of bone scaffold materials, the use of composites has been widely explored. The use of ceramic materials such as tricalcium phosphates, hydroxyapatite (HAP), or bioactive glass as inclusions in polymer matrices is often used to enhance mechanics (9, 11–13). Similarly, studies using reinforcing silk particles (fabricated by milling) into a silk matrix resulted in improved scaffolds for bone applications with compressive properties in hydrated state of approximately 3 MPa, improving the ingrowth of human bone marrow-derived mesenchymal stem cells (hMSCs) in vitro toward forming bone-like tissues (14–16).

Currently, bone graft/scaffold engineering using silk biomaterials has received increasing interest as an alternative option (14, 15, 17, 18). However, toward, this goal several biological parameters need to be met including biocompatibility, biodegradability, surface roughness, porosity, osteoconductivity, and above all high mechanical integrity (4, 14, 15). However, many challenges remain to satisfy an optimally functional bone regeneration scaffold system (19). Perhaps the biggest challenge is the need for polymer biomaterials to meet the high compressive properties of bone, a prerequisite to function in vivo (14, 15, 20).

Silk fibroin from *Bombyx mori* was chosen as the protein for the current study due to its desirable properties including biocompatibility with low inflammatory and immunogenic responses (17, 18, 21–25). The unique β-sheet (crystalline)-rich structure imparts high stiffness and toughness to silk biomaterials, making it a useful biopolymer for bone engineering applications (23). In our prior studies we reported ultimate tensile strength values between 610 and 690 MPa for silk filaments, compared to 0.9–7.4 MPa for rattail-type I collagen and 28–50 MPa for polylactic acid (PLA), respectively (23). Similarly, a modulus between 15 and 17 GPa for silk was reported and compared to 0.0018–0.046 GPa, for collagen, and 1.2–3.0 GPa for PLA (19). Silk has achieved US Food and Drug Administration approval for some medical devices. Additionally, due to the amphiphilic features, postprocessing of silk into various material formats including films, scaffolds, fibers, hydrogels, and sponges is feasible with tunable degradation properties for biomaterial and tissue engineering applications (21, 22, 26).

In the present study, the goal was to improve the compressive properties of silk scaffolds to match the requirements for bone. The approach was to exploit silk microfiber reinforcements as a step toward orthopedic biomaterials for repairs. Toward this goal, a unique silk hydrolysis method was developed to fabricate micron-sized silk fibers as fillers with a silk matrix for reinforcement. The effects of fiber length and content on compressive properties of these unique silk protein-protein composite materials were investigated based on the strong protein-protein interfacial bonding between the two silk phases. Subsequent studies focused on the compatibility of these systems for hMSC differentiation for bone tissue engineering applications.

Results and Discussion

Previous in vivo and in vitro studies using porous silk scaffolds have shown potential toward reconstruction of bone and bone-related grafts due to the intrinsic high mechanical strength and robustness (17, 18, 21, 22, 26, 27). However, greater strength was desired to match bone requirements, thus newer strategies would not only help to reduce bone graft failures but would also provide an alternate option of using scaffolds as direct load-bearing supports to improve in vivo tissue engineering outcomes. To progress toward this goal of high-strength silk scaffolds, in this study a simpler method to achieve micron range fibers from degummed silk by alkali hydrolysis was identified. Subsequently these different sized (10–500 μm) silk microfibers were used to reinforce silk scaffolds, with the added benefit of the ability to

Author contributions: B.B.M. and D.L.K. designed research; B.B.M., A.G., E.S.G., and B.P. performed research; B.B.M. contributed new reagents/analytic tools; B.B.M., A.G., E.S.G., B.P., and D.L.K. analyzed data; and B.B.M. and D.L.K. wrote the paper.

The authors declare no conflict of interest.

This article is a PNAS Direct Submission.

[1]To whom correspondence should be addressed. E-mail: david.kaplan@tufts.edu.

This article contains supporting information online at www.pnas.org/lookup/suppl/doi:10.1073/pnas.1119474109/-/DCSupplemental.

control microfiber size and particle loading to investigate impact on mechanical properties toward bone tissue engineering.

Silk-Fiber Formation. Alkaline hydrolysis of proteins is a well-documented procedure. However, to our knowledge use of this process to generate microfibers from native silk fibers for reinforcement studies was unique, in that we could modulate and control the size of the microfibers obtained using a faster (in seconds) and cost-effective method compared with expensive and time-consuming conventional ball-and-jet milling methods (Fig. 1, Fig. 2) (16, 28, 29). The length of silk microfibers obtained in the process was inversely proportional to time of hydrolysis (Fig. 2*A*). The alkali (sodium hydroxide) initiates hydrolysis of amide bonds by conversion to a carboxylic acid and an amine or ammonia, which can be smelled during the reaction. Hydrolysis was faster with random chopping during the initial 0–15 s but became steady over time. After the initial 15 s, the average microfiber length obtained was 354 ± 84 μm, which dropped to 263 ± 67, and 191 ± 46 μm after 50 and 70 s, respectively (Fig. 2*A*). What is particularly interesting is the stepwise decrease in silk microfiber length, perhaps accounted for by the specific arrangement of the beta-sheets (crystallites) and less crystalline regions within the silk structure (30) (Fig. 1*B*). We can hypothesize that there is a sequential hydrolysis of silk regions more prone to the reaction, such as the noncrystalline domains. Some amino acids of silk [e.g., arginine (1% in silk) and serine (13% in silk)] are destroyed in the process, but others are racemized (31). This finding is further supported by the rapid exothermic hydrolysis reaction resulting in smaller microfibers in the 1,000 μm range within 5–10 s (Fig. 2*A*). Similarly, slowing down of the hydrolysis process as observed from the microfiber sizes obtained after the initial 15–20 s may be attributed to cleaving the more crystalline regions of the silk, due to the stronger hydrogen bonding, resulting in finer fibers (150–300 μm fibers between 50–720 s) (Fig. 1*B*, Fig. 2*I*). Further, upon supply of external heat (energy to break the bonds) faster hydrolysis with finer fibers of 10 ± 5 μm size was observed, presumably due to rapid cleaving of both less crystalline and crystalline silk regions (Fig. 1*C*) (30). In approximately 60 s, microfibers ranging 10–20 μm were obtained as compared to 100-μm plus-sized fibers after 720 s of normal reaction without external heating (Fig. 2*A*). This slight modification allowed us to fabricate a wider range of microfiber sizes of which three different groups, 10–20, 150–200, and 400–500 μm, were selected and designated as small, medium, and large microfibers, respectively, for the silk-fiber scaffold reinforcement studies reported here (Fig. 1*C*). However, during the course of hydrolysis fiber diameter was observed to remain within a range of 10 ± 2 μm except for hydrolysis with external heating where the fibers were fragmented to various smaller sizes (Fig. 1 *B* and *C*).

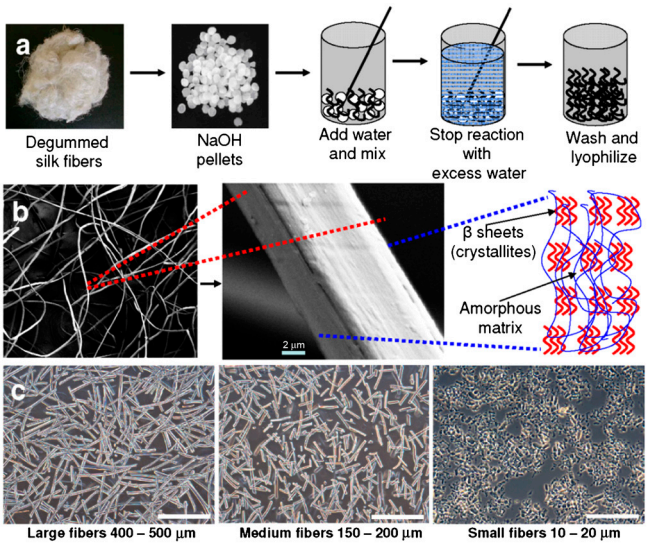

Fig. 1. (*A*) Schematic representation of silk-fiber fabrication steps, (*B*) SEM image showing degummed silk-fiber morphology and possible arrangements of crystalline and less crystalline domains, and (*C*) hydrolyzed silk microfibers of varied lengths used as fillers for fabricating reinforced scaffolds. (Scale bar, 400 μm.)

Reinforced Silk Scaffold Fabrication. To fabricate microfiber-reinforced silk scaffolds, 25 wt % hexafluoroisopropanol (HFIP) silk solution was blended with equal amounts (1:1, HFIP:silk microfiber) or three times more microfibers by wt % (1:3, HFIP:silk-fiber). Similarly, HFIP-silk alone (25 wt %) was used to fabricate control scaffolds (without microfibers). In each ratio, three different types of reinforced scaffolds were fabricated using microfibers of larger (400–500 μm), medium (150–200 μm), and smaller (10–20 μm) lengths (Fig. 1*C*). Strong interfacial contact between blended polymers within a composite is critical for achieving higher stiffness (14, 32). Following a similar principle, silk was chosen as the common material for both the phases (fiber and bulk matrix) to achieve enhanced interfacial protein-protein compatibility as evident from the SEM images. By external observation, 1:1 scaffolds appeared more porous than 1:3 ratio scaffolds (Fig. 3). However, 1:3 ratio scaffolds were rougher in appearance compared to the 1:1 scaffolds. Porosity as calculated by the liquid (hexane) displacement method was approximately 88 ± 09, 82 ± 11, and 77 ± 08% for the reinforced scaffolds with larger, medium, and smaller microfibers, respectively, in the 1:1 ratio. For 1:3 ratios, the scaffold porosities decreased to 81 ± 08, 73 ± 10, and 69 ± 7% for the larger, medium, and smaller microfibers, respectively. In comparison, control HFIP-silk scaffolds showed the highest porosity of 90 ± 13%. However, control scaffolds had thicker walls between pores in comparison to the microfiber scaffolds, which had open-ended, highly porous walls as evident from SEM (Fig. 3). Further, no evidence of phase separation was observed, demonstrating miscibility of silk microfibers with the silk matrix toward a strong composite via optimal interfacial contact (Fig. 3) (32).

Comparing SEM images, it is evident that the overall surface roughness, including the roughness of pore walls and interconnectivity, increased for both ratios of 1:1 and 1:3 upon the addition of larger microfibers when compared to smaller fibers, with an average pore size in the range of 500–600 μm (Fig. 3). Medium fibers showed an intermediate roughness, and smaller fibers had a more compact structure with less fibrous solid walls (Fig. 3). Bonded silk fibers can be seen intertwined throughout the scaffold making the surface rough and porous with good miscibility (14). This enhancement of roughness is an added advantage for these new composite scaffolds as interconnected porous structures are important for new bone tissue regeneration, allowing integration via adequate neovascularization and nutrient/metabolic waste diffusion (19, 27, 33). Further, using salt leaching, control over the range of pore sizes and geometry can be attained by choosing the appropriate salt grain size (in this study 800 μm grains were used) to mimic bone features related to distinct anatomical bone sites (34, 35).

Biomechanics. High mechanical stability is a prerequisite for load-bearing biomedical implants, especially for bone tissue engineering to withstand high compressive in vivo stresses. Although silk in its natural fiber form is considered a ductile and stiff polymer, its postprocessing and fabrication steps determine scaffold mechanical properties. In an attempt to achieve high compressive properties, silk microfibers were used in the present study as fillers along with a bulk silk matrix to achieve high-strength composite scaffolds. Use of such reinforcing fillers is a preferred

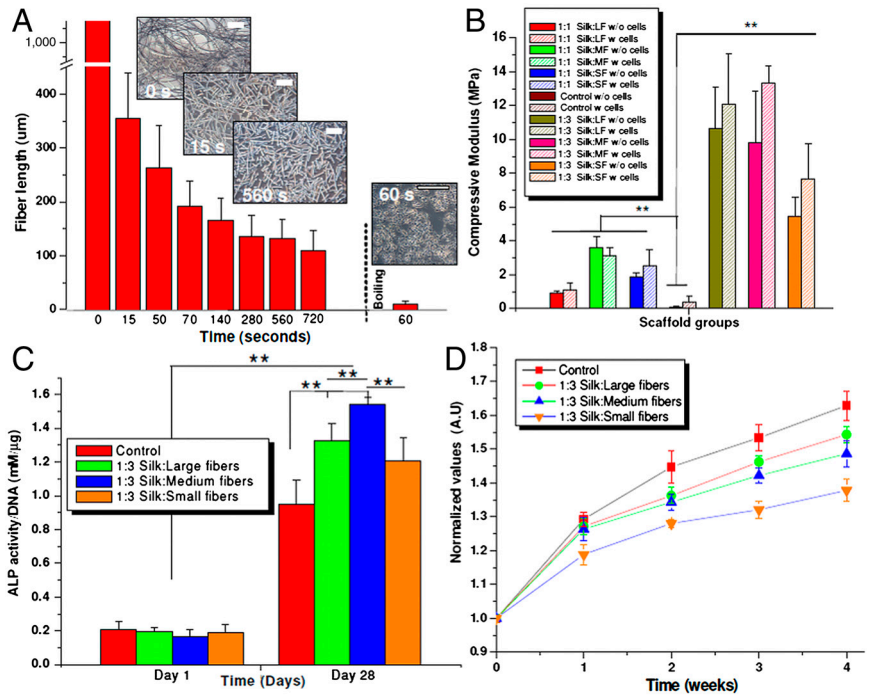

Fig. 2. (*A*) Varied lengths of silk microfibers obtained after alkali hydrolysis, (*B*) compressive modulus of silk microfiber-reinforced scaffolds of ratios 1:1 and 1:3, before and after cell culture (28 d), (*C*) ALP activity of seeded hMSCs under differentiating conditions on silk microfiber-reinforced scaffolds, and (*D*) cell proliferation showing normalized values of cell growth within silk scaffolds over a period of 4 wk. (Scale bar, 200 μm.) Data represents mean ± standard deviation ($n = 5$), where $^{**}P \leq 0.01$ and $^{*}P \leq 0.05$.

approach in engineering to enhance composite strength and has been reported for silk (14, 16, 36, 37).

Following testing in a hydrated state, acellular scaffolds of 1:3 ratios were found to be 4–5 times the modulus when compared to the 1:1 scaffolds (Fig. 2*B*). Due to higher fiber density in the 1:3 ratio, the modulus of the scaffolds with larger microfibers increased from 0.90 ± 0.11 to 10.64 ± 2.46 MPa ($^{**}P \leq 0.01$).

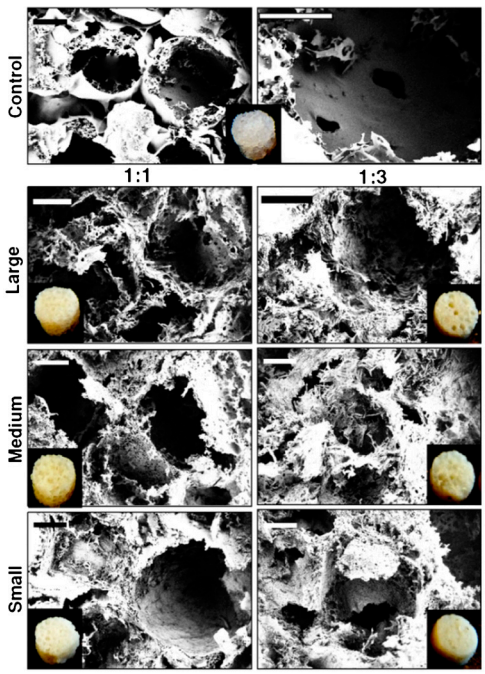

Fig. 3. SEM images showing silk scaffold characteristics including pore size, microfiber bonding, porosity, and surface roughness. *Inset* shows fabricated scaffold used for cell culture. (Scale bar, 200 μm.)

Similarly for scaffolds containing the medium and small microfibers, the values were enhanced from 3.62 ± 0.65 and 1.86 ± 0.21 to 9.79 ± 3.05 and 5.42 ± 1.18 MPa, respectively ($^{**}P \leq 0.01$). An approximate increase of 9.70, 6.10, and 3.50 MPa, respectively, for scaffolds reinforced with large, medium, and small microfibers (Fig. 2*B*). In comparison, control HFIP-silk scaffolds showed much lower modulus of 85.06 ± 32.62 kPa ($^{**}P \leq 0.01$). Because of the strong protein-protein cohesive bonding, higher compressive modulus values were achieved in fiber-bonded scaffolds (acellular) when compared to control HFIP-silk scaffolds (50–100-fold increase) (Fig. 2*B*). Interestingly, differences in compressive properties were observed with the different sized microfibers as well as the change silk-fiber content (Fig. 2*B*). Understandably, higher fiber amounts (1:1 vs. 1:3 ratios) led to greater packing density, yielding stronger composites with higher mechanical properties (14, 16). However, using a similar fiber content (1:3 ratio), comparable high compressive values were obtained for scaffolds with the larger and medium fibers, in the range of approximately 10 MPa in the hydrated state (these values represent the strongest silk scaffolds to date), possibly due to the improved bonding of microfibers to the matrix as observed from SEM (Fig. 3). Further, these longer microfibers possibly help to bind better to the silk matrix by partial dissolution in the presence of HFIP (14). This binding in turn will help with more effective transfer of load during compression from the matrix to the reinforcement and help eliminate stress buildup, resulting in increased toughness and strength (16, 38). In comparison, smaller microfibers (with similar fiber content of 1:3) due to their short sizes, fail to make a larger connected composite mat, resulting in ineffective transfer of load during compression, and yielding lower compressive values (Fig. 3).

Studies using partially dissolved polyphosphazene have shown a similar effect after binding to nano-hydroxyapatite forming stronger reinforced scaffolds (39). Our results are in line with previous silk reinforcement studies using 1–5 μm silk particles obtained through milling, yielding compressive values of approximately 2.8 MPa under hydrated conditions (one-fourth of our

current values), confirming the role of fiber size/length on compressive properties (14, 16). In comparison, control HFIP scaffolds without microfibers showed lower compressive values of approximately 85 kPa, related to the presence of intermolecular hydrogen bonds between silk chains in the β-sheets induced due to methanol treatment (14, 16, 40). Utilizing these weaker hydrogen bonds within β-sheet nanocrystals, nanoconfinement of such smaller β-sheet nanocrystals in silk achieved higher stiffness, strength, and mechanical toughness as elucidated previously (41, 42). In combination with inherent silk-fiber strength, compact fiber reinforcement led to enhanced compressive properties within the scaffolds.

When used in lower proportions to the silk matrix (as in 1:1 ratios), silk scaffolds with microfibers of larger size showed contrasting results (Fig. 2*B*). This behavior is possibly due to uneven packing, where smaller- and medium-sized microfibers, due to their greater numbers in comparison to the larger microfibers, distributed better, resulting in more even packing and stronger composites (~2–4 MPa) in contrast to larger microfibers (~1 MPa), which can leave gaps (observed during sectioning) resulting in lower compressive properties.

The importance of the high compressive data in the 1:3 ratio study group (in the hydrated state) is emphasized when compared with previously reported conventional degradable polymeric biomaterials like collagen, PCL, PLGA, chitosan, and gelatin intended for bone tissue engineering. Collagen in pure form is known to have low compressive properties in the hydrated state (2–150 kPa) and even in blends with osteoinductive hydroxyapatite (HA) and bioglass, porous scaffolds have shown low compressive properties in the range of 200 kPa and 2.97 MPa, respectively (43, 44). Further, using 4.8 wt % chitosan, 2.56 MPa was reached in scaffolds, and in combination with alginate (in equal ratios) there was an increase to 8.1 MPa when tested in the dry state (45). Similarly, PCL/HA and PLGA/β-tricalcium phosphate (β-TCP) scaffolds had values of 0.74 and 4.19 MPa, respectively, much lower than our current values with biodegradable silk scaffolds in the hydrated state (46, 47).

Further, a possible role of ECM toward mechanical improvements was evaluated using silk-fiber-reinforced scaffolds by culturing and differentiating hMSCs toward bone-like tissue. Enhanced biomechanics were observed due to possible deposition of ECM and mineralization as a result of osteogenic differentiation within scaffolds of all ratios and types over time [higher collagen, alkaline phosphatase (ALP) gene expression]. Our result agrees with previous studies using hMSCs on silk scaffolds toward enhanced biomechanics (15, 48, 49). With an increase of approximately 26%, compressive moduli of scaffolds with medium-sized microfibers reached a maximum of approximately 13 MPa followed by large and smaller sized microfiber scaffolds with enhancement of approximately 12% (~11 MPa), and approximately 29% in compressive modulus (~7.5 MPa), respectively (Fig. 2*B*). No statistical difference was observed between compressive values of larger and medium microfiber scaffolds. However, we expect compressive values to enhance further in longer cultures greater than the current study of 4 wk.

Human Bone Marrow Stem Cell Proliferation and Osteogenesis. Although significant improvements in compressive properties (~13 MPa) was observed, exceeding values needed for cancellous bone (~10 MPa), still these values are significantly lower than that of native cortical bone (~100 MPa) (14, 16, 28). Toward achieving such mechanical properties, we hypothesize to use these unique composite scaffolds as temporary, biodegradable support conduits for native cells to grow and replace with ECM, thus improving biomechanical properties over time. Cellular proliferation, osteogenic potential and in vivo compatibility were investigated. As compared to day 0 (seeding day), cells proliferated with time (Fig. 2*D*). From plotted normalized values, proliferation rate was steady after week one and two, possibly due to induction of osteogenesis within the scaffolds. Cell proliferation (normalized) was highest within the scaffolds in the control HFIP-silk scaffolds followed by the reinforced scaffolds with larger and medium microfibers, then lowest in case of smaller microfibers (Fig. 2*B*). In comparison to the controls, at the end of week four, the scaffolds with smaller microfibers showed approximately 15% fewer cells followed by approximately 4% and approximately 8% in the case of the larger and medium-sized microfiber scaffolds, respectively. The lower cell proliferation on microfiber scaffolds compared to controls may be due to lower

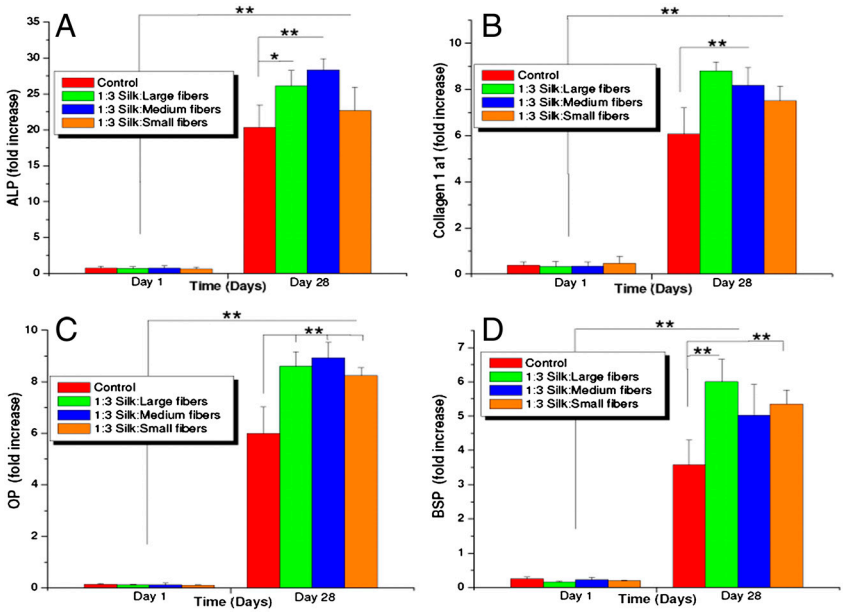

Fig. 4. Real-time gene expression conducted on silk microfiber-reinforced scaffolds seeded with hMSCs under differentiating conditions showing fold expression of osteogenic genes: (*A*) ALP, (*B*) Collagen 1a1, (*C*) OP, and (*D*) BSP. (Scale bar, 200 μm.) Data represents mean ± SD ($n = 4$), where $^{**}P \leq 0.01$ and $^{*}P \leq 0.05$.

porosity, hindering cell migration, and may be optimized using bigger salt granules during fabrication (Fig. 2*D*) (50).

In the present study, we observed hMSC differentiation (higher transcript levels of osteogenic markers) toward bone-like cells at an increased rate on the more rigid and rougher fiber-reinforced scaffolds when compared to the controls ($^{**}P \leq 0.01$) (Fig. 2*C*, Fig. 4) (15, 49). Seeded cells grew and proliferated with significant expression (sixfold to ninefold after day 28) of collagen (Collα1) within the microfiber-reinforced scaffolds, similar to controls ($^{**}P \leq 0.01$) (Fig. 4). Significant increases in levels (sixfold to ninefold) of osteopontin (OP) and bone sialoprotein (BSP) (fourfold to sixfold) were observed on day 28 for the microfiber-reinforced scaffolds as compared to HFIP-controls, a sign of enhanced osteogenesis ($^{**}P \leq 0.01$) (15, 18, 49). Similarly, ALP activity increased 20- to 30-fold, including controls, when compared to day 1, with the highest expression observed in the case of scaffolds with the medium-sized microfibers, followed by larger and smaller microfibers, respectively ($^{**}P \leq 0.01$) (Fig. 4).

It is not surprising that with increased roughness and rigidity of scaffolds an enhancement of hMSC differentiation toward bone was observed. A role of matrix stiffness and surface roughness in cell motility and behavior has been explored and reported to influence differentiation (51–53). Particularly, hMSCs differentiating into an osteogenic lineage on stiffer matrices has been reported, including studies on three-dimensional silk matrices (15, 17, 18, 49, 52–54). Higher OP and BSP transcript levels are indicative of the maturity of the mineralized matrix where OP is specifically responsible for cell attachment at bone modeling sites, regulation of crystal formation, and growth due to its ability to bind to hydroxyapatite, whereas, BSP enhances nucleation of hydroxyapatite crystals and is a marker for osteogenesis (55, 56). Higher levels of ALP, a marker for osteoblastic phenotype, further confirm enhanced differentiation of hMSCs on reinforced scaffolds when compared to the controls (49, 52, 53).

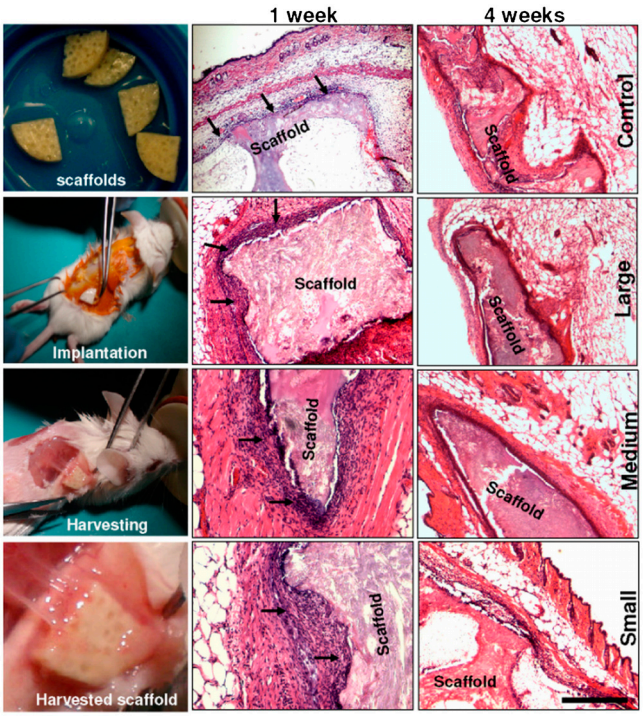

Fig. 5. Histological images showing in vivo immunological response of fabricated silk microfiber scaffolds in mice. Sample sections were stained with H&E. Microscopic images (*Left*) show scaffolds implanted subcutaneously in mice and a harvested highly vascularized implant after 4 wk.

In Vivo Responses. To better understand material immune response and implant integration, the fabricated scaffolds (both tests and controls) were implanted into mice subcutaneously at the back and were retrieved after 1 and 4 wk (Fig. 5). Following retrieval of scaffolds after week 1 and H&E staining, inflammatory cells (mainly macrophages marked with arrows) were observed surrounding the implanted scaffolds of all types, a sign of milder, more indolent tissue reaction and a more compact zone of repair (24, 57). On close observation, the number of inflammatory cells surrounding the control, larger, and medium microfiber scaffolds were less compared to the cells with the smaller microfiber-reinforced scaffolds (Fig. 5). One explanation for these differences could be associated with the size of the foreign materials (10–20 μm silk fibers) inducing greater adhesion and effective phagocytosis by surrounding macrophages compared to larger particles less susceptible to phagocytosis (58). Medium microfiber scaffolds showed intermittent numbers of inflammatory cells. The layer of macrophages and fibroblasts were 4–5 cell sheets thick and the macrophages were restricted to the immediate host-implant interface. The interface layer was superimposed by oriented fibroblasts and rare lymphocytes, and was devoid of giant cells. However, around the scaffolds with the smaller microfibers higher numbers of macrophages, plasma cells, and increased vascularization was present at the rougher surface areas of the scaffolds. The layer of macrophages, fibroblasts, and plasma cells was 8–12 cell sheets thick (Fig. 5). Silk degradation was not visibly observed over the time frame of study.

Following a four-week study, dense tissue ingrowth with vascularization surrounding the implants was observed (Fig. 5). The retrieved scaffold samples showed fewer inflammatory cells surrounding the implants in all scaffold samples including the scaffolds with the smaller microfibers, with close integration of the implants and mice tissue (Fig. 5). This observation is supported by previous reports showing less adhesion of immunocompetent cells to pure silk fibroin in vitro, compared to polystyrene and poly(2-hydroxyethyl methacrylate) (57). Similarly, studies with silk nonwoven mats implanted subcutaneously in rats induced a weak foreign body response and no fibrosis with little upregulation of inflammatory pathways at the implantation site and no invasion by lymphocytes after 6 mo in vivo (25). Further, immune compatibility of pure silk films has already been demonstrated in vivo, inducing a lower inflammatory response than collagen films and PLA films (24).

Conclusions

A unique method to generate silk microfibers with control of length was demonstrated. As a result, silk microfiber-reinforced three-dimensional scaffolds were fabricated with strong protein-protein interfacial bonding between the microfiber and bulk silk components resulting in promising compressive properties. The developed three-dimensional-scaffold systems provided insight on the role of microfiber dimensions on mechanical properties and immune responses. Further, silk microfiber-protein composite matrices mimicked the mechanical features of native bone including matrix stiffness and surface roughness favoring enhanced hMSC differentiation compared to control silk sponges. Together, this study may aid development of high-strength biopolymeric scaffolds toward tissue engineering of bone.

Materials and Methods

Silk Scaffold Fabrication. *Bombyx mori* aqueous silk and 25% (wt/vol) HFIP-silk solution was prepared as described previously (14, 48). Varied sized silk fibers (10–500 μm) were fabricated from degummed silk after alkali hydrolysis followed by reinforcement using HFIP-silk in ratios of 1:1 and 1:3 (fiber:silk solution).

Biophysical and Biochemical Studies. Scaffold morphology was evaluated using SEM and porosity by liquid displacement method (14). For biomechanical evaluation, acellular and cellularized scaffolds were tested using Instron

3366 at physiological condition. DNA, ALP, Alamar blue and real-time gene expression studies for collagen type Iα (Col Iα1), ALP, BSP, and OP were performed following manufacturer's protocol.

In Vivo Studies. The balb/c female mice were used following protocols approved by Tufts Institutional animal care and use committee. Scaffolds were implanted subcutaneously under general anesthesia. Inflammatory responses were checked at end of 1 and 4 wk after H&E staining. A more detailed description is included in *SI Materials and Methods*.

Statistical Analysis. All quantitative experiments were run at least in triplicate (unless specified), and results are expressed as mean ± standard deviation. Statistical analysis of data was performed by one-way ANOVA. Differences between groups of $*P \leq 0.05$ were considered statistically significant and $**P \leq 0.01$ was considered highly significant.

ACKNOWLEDGMENTS. We thank the Air Force Office of Scientific Research. This work was supported by National Institutes of Health Grants DE017207, EB003210, and EB002520. .

1. Drosse I (2008) Tissue engineering for bone defect healing: An update on a multi-component approach. *Injury* 39(Suppl 2):S9–S20.
2. Langer R, Vacanti JP (1993) Tissue engineering. *Science* 260:920–926.
3. Marquis ME, et al. (2009) Bone cells biomaterials interactions. *Front Biosci* 14:1023–1067.
4. Khan Y, Yaszemski MJ, Mikos AG, Laurencin CT (2008) Tissue engineering of bone: Material and matrix considerations. *J Bone Joint Surg Am* 90:36–42.
5. Dawson JI, et al. (2008) Development of specific collagen scaffolds to support the osteogenic and chondrogenic differentiation of human bone marrow stromal cells. *Biomaterials* 29:3105–3116.
6. Oliveira JM, et al. (2006) Novel hydroxyapatite/chitosan bilayered scaffold for osteochondral tissue engineering applications: Scaffold design and its performance when seeded with goat bone marrow stromal cells. *Biomaterials* 27:6123–6137.
7. Le Nihouannen D, et al. (2006) Micro-architecture of calcium phosphate granules and fibrin glue composites for bone tissue engineering. *Biomaterials* 27:2716–2722.
8. Ochi K, et al. (2003) Use of isolated mature osteoblasts in abundance acts as desired-shaped bone regeneration in combination with a modified poly-DL-lactic-co-glycolic acid (PLGA)-collagen sponge. *J Cell Physiol* 194:45–53.
9. Zhang K, Ma Y, Francis LF (2002) Porous polymer/bioactive glass composites for soft to hard tissue interfaces. *J Biomed Mater Res* 61:551–563.
10. Hutmacher DW, et al. (2001) Mechanical properties and cell cultural response of polycaprolactone scaffolds designed and fabricated via fused deposition modeling. *J Biomed Mater Res* 55:203–216.
11. Thein-Han WW, Shah J, Misra RD (2009) Superior in vitro biological response and mechanical properties of an implantable nanostructured biomaterial: Nano hydroxyapatite-silicone rubber composite. *Acta Biomater* 5:2668–2679.
12. Wei GB, Ma PX (2004) Structure and properties of nano-hydroxyapatite/polymer composite scaffolds for bone tissue engineering. *Biomaterials* 25:4749–4757.
13. Zhang Y, Wu C, Friis T, Xiao Y (2010) The osteogenic properties of CaP/silk composite scaffolds. *Biomaterials* 31:2848–2856.
14. Gil ES, et al. (2011) Mechanical improvements to reinforced porous silk scaffolds. *J Biomed Mater Res Part A* 99:16–28.
15. Rockwood DN, et al. (2011) Ingrowth of human mesenchymal stem cells into porous silk particle reinforced silk composite scaffolds: An in vitro study. *Acta Biomater* 7:144–151.
16. Rajkhowa R, et al. (2010) Reinforced silk scaffolds with silk particles. *Macromol Biosci* 10:599–611.
17. Mandal BB, Kundu SC (2009) Non-mulberry silk gland fibroin 3D scaffold for enhanced differentiation of human mesenchymal stem cells into osteocytes. *Acta Biomater* 5:2579–2590.
18. Mandal BB, Kundu SC (2009) Osteogenic and adipogenic differentiation of rat bone marrow cells on mulberry and non-mulberry silk gland fibroin 3D scaffolds. *Biomaterials* 30:5019–5030.
19. Salgado AJ, Coutinho OP, Reis RL (2004) Bone tissue engineering: State of the art and future trends. *Macromol Biosci* 4:743–765.
20. Zhou YF, et al. (2007) Combined marrow stromal cell-sheet techniques and high strength biodegradable composite scaffolds for engineered functional bone grafts. *Biomaterials* 28:814–824.
21. Omenetto FG, Kaplan DL (2010) New opportunities for an ancient material. *Science* 329:528–531.
22. Wang Y, Kim HJ, Vunjak-Novakovic G, Kaplan DL (2006) Stem cell-based tissue engineering with silk biomaterials. *Biomaterials* 27:6064–6082.
23. Altman GH, et al. (2002) Silk matrix for tissue engineered anterior cruciate ligaments. *Biomaterials* 23:4131–4141.
24. Meinel L, et al. (2005) The inflammatory responses to silk films in vitro and in vivo. *Biomaterials* 26:147–155.
25. Dal Pra I, Freddi G, Minic J, Chiarini A, Armato U (2005) De novo engineering of reticular connective tissue in vivo by silk fibroin nonwoven materials. *Biomaterials* 26:1987–1999.
26. Wang Y, et al. (2008) In vivo degradation of three-dimensional silk fibroin scaffolds. *Biomaterials* 29:3415–3428.
27. Kim HJ, et al. (2007) Bone regeneration on macroporous aqueous-derived silk 3-D scaffolds. *Macromol Biosci* 7:643–655.
28. Rajkhowa R, Wang L, Wang X (2008) Ultrafine silk powder preparation through rotary and ball milling. *Powder Technol* 185:87–95.
29. Rajkhowa R, Wang L, Kanwar J, Wang X (2009) Fabrication of ultrafine powder from eri silk through attritor and jet milling. *Powder Technol* 191:155–163.
30. Shao ZZ, Vollrath F (2002) The surprising strength of silkworm silk. *Nature* 418:741.
31. Coleman D, Howitt FO (1947) Studies on silk proteins. I. The properties and constitution of fibroin. The conversion of fibroin into a water-soluble form and its bearing on the phenomenon of denaturation. *Proc R Soc Lond A Math Phys Sci* 190:145–169.
32. Desai AV, Haque MA (2005) Mechanics of the interface for carbon nanotube-polymer composites. *Thin-Walled Struct* 43:1787–1803.
33. Kim HJ, Kim UJ, Vunjak-Novakovic G, Min BH, Kaplan DL (2005) Influence of macroporous protein scaffolds on bone tissue engineering from bone marrow stem cells. *Biomaterials* 26:4442–4452.
34. Hodgskinson R, Currey JD (1992) Young modulus, density and material properties in cancellous bone over a large density range. *J Mater Sci Mater M* 3:377–381.
35. Müller R, et al. (1998) Morphometric analysis of human bone biopsies: A quantitative structural comparison of histological sections and micro-computed tomography. *Bone* 23:59–66.
36. Ramakrishna S, Mayer J, Wintermantel E, Leong KW (2001) Biomedical applications of polymer-composite materials: A review. *Compos Sci Technol* 61:1189–1224.
37. Lau KT, Gu C, Hui D (2006) A critical review on nanotube and nanotube/nanoclay related polymer composite materials. *Compos Part B Eng* 37:425–436.
38. Wang M (2003) Developing bioactive composite materials for tissue replacement. *Biomaterials* 24:2133–2151.
39. Nukavarapu SP, et al. (2008) Polyphosphazene/nano-hydroxyapatite composite microsphere scaffolds for bone tissue engineering. *Biomacromolecules* 9:1818–1825.
40. Nazarov R, Jin HJ, Kaplan DL (2004) Porous 3-D scaffolds from regenerated silk fibroin. *Biomacromolecules* 5:718–726.
41. Keten S, Xu Z, Ihle B, Buehler MJ (2010) Nanoconfinement controls stiffness, strength and mechanical toughness of β-sheet crystals in silk. *Nat Mater* 9:359–367.
42. Nova A, Keten S, Pugno NM, Redaelli A, Buehler MJ (2010) Molecular and nanostructural mechanism of deformation, strength and toughness of spider silk fibrils. *Nano Lett* 10:2626–2634.
43. Kane RJ, Roeder RK (2011) Effects of hydroxyapatite reinforcement on the architecture and mechanical properties of freeze-dried collagen scaffolds. *J Mech Behav Biomed Mater*, 10.1016/j.jmbbm.2011.09.010.
44. Xu C, et al. (2011) Biocompatibility and osteogenesis of biomimetic bioglass-collagen-phosphatidylserine composite scaffolds for bone tissue engineering. *Biomaterials* 32:1051–1058.
45. Li Z, Ramay HR, Hauch KD, Xiao D, Zhang M (2005) Chitosan-alginate hybrid scaffolds for bone tissue engineering. *Biomaterials* 26:3919–3928.
46. Kang Y, et al. (2011) Enhanced mechanical performance and biological evaluation of a PLGA coated β-TCP composite scaffold for load-bearing applications. *Eur Polym J* 47:1569–1577.
47. Wang Y, Dai J, Zhang Q, Xiao Y, Lang M (2010) Improved mechanical properties of hydroxyapatite/poly(caprolactone) scaffolds by surface modification of hydroxyapatite. *Appl Surf Sci* 256:6107–6112.
48. Mandal BB, Park SH, Gil ES, Kaplan DL (2011) Multilayered silk scaffolds for meniscus tissue engineering. *Biomaterials* 32:639–651.
49. Park SH, Gil ES, Kim HJ, Lee K, Kaplan DL (2010) Relationship between degradability of silk scaffolds and osteogenesis. *Biomaterials* 31:6162–6172.
50. Mandal BB, Kundu SC (2009) Cell proliferation and migration in 3D silk fibroin scaffolds. *Biomaterials* 30:2956–2965.
51. Discher DE, Janmey P, Wang YL (2005) Tissue cells feel and respond to the stiffness of their substrate. *Science* 310:1139–1143.
52. Balloni S, et al. (2009) Effects of titanium surface roughness on mesenchymal stem cell commitment and differentiation signaling. *Int J Oral Maxillofac Implants* 24:627–635.
53. Hu X, et al. (2011) The influence of elasticity and surface roughness on myogenic and osteogenic-differentiation of cells on silk elastin biomaterials. *Biomaterials* 32:8979–8989.
54. Engler AJ, Sen S, Sweeney HL, Discher DE (2006) Matrix elasticity directs stem cell lineage specification. *Cell* 126:677–689.
55. Giachelli CM, Steitz S (2000) Osteopontin: A versatile regulator of inflammation and biomineralization. *Matrix Biol* 19:615–622.
56. Ganss B, Kim RH, Sodek J (1999) Bone sialo protein. *Crit Rev Oral Biol Med* 10:79–98.
57. Santin M, Motta A, Freddi G, Cannas M (1999) In vitro evaluation of the inflammatory potential of the silk fibroin. *J Biomed Mater Res* 46:382–389.
58. Jutras I, Desjardins M (2005) Phagocytosis: At the crossroads of innate and adaptive immunity. *Annu Rev Cell Dev Biol* 21:511–527.